Structure, Vol. 8, 1137–1146, November, 2000, ©2000 Elsevier Science Ltd. All rights reserved. PII S0969-2126(00)00529-3

Crystal Structure of the Human Acyl Protein Thioesterase I from a Single X-Ray Data Set to 1.5 Å

Yancho Devedjiev,* Zbigniew Dauter,† Sergey R. Kuznetsov,‡ Teresa L. Z. Jones,‡ and Zygmunt S. Derewenda*§

*Department of Molecular Physiology and Biological Physics
University of Virginia
Health Sciences System
Charlottesville, Virginia 22908
†National Cancer Institute
Frederick and National Brookhaven Laboratory
Upton, New York 11973
‡Metabolic Diseases Branch
National Institute of Diabetes and Digestive and Kidney Diseases
National Institutes of Health
Bethesda, Maryland 20892

Summary

Background: Many proteins undergo posttranslational modifications involving covalent attachment of lipid groups. Among them is palmitoylation, a dynamic, reversible process that affects trimeric G proteins and Ras and constitutes a regulatory mechanism for signal transduction pathways. Recently, an acylhydrolase previously identified as lysophospholipase has been shown to function as an acyl protein thioesterase, which catalyzes depalmitoylation of Gα proteins as well as Ras. Its amino acid sequence suggested that the protein is evolutionarily related to neutral lipases and other thioesterases, but direct structural information was not available.

Results: We have solved the crystal structure of the human putative Gα-regulatory protein acyl thioesterase (hAPT1) with a single data set collected from a crystal containing the wild-type protein. The phases were calculated to 1.8 Å resolution based on anomalous scattering from Br^- ions introduced in the cryoprotectant solution in which the crystal was soaked for 20 s. The model was refined against data extending to a resolution of 1.5 Å to an R factor of 18.6%. The enzyme is a member of the ubiquitous α/β hydrolase family, which includes other acylhydrolases such as the palmitoyl protein thioesterase (PPT1).

Conclusions: The human APT1 is closely related to a previously described carboxylesterase from *Pseudomonas fluorescens*. The active site contains a catalytic triad of Ser-114, His-203, and Asp-169. Like carboxylesterase, hAPT1 appears to be dimeric, although the mutual disposition of molecules in the two dimers differs. Unlike carboxylesterase, the substrate binding pocket and the active site of hAPT1 are occluded by the dimer interface, suggesting that the enzyme must dissociate upon interaction with substrate.

§To whom correspondence should be addressed (e-mail: zsd4n@virginia.edu).

Introduction

Proteins involved in signal transduction and cell regulation often function at the cell membrane. Some, like G protein–coupled receptors, are integral, but many others are thought to interact with the phospholipid bilayer transiently with the aid of posttranslationally attached lipid moieties. These chemical modifications are increasingly appreciated for their physiological significance; they include prenylation, specific for the cysteine within the CAAX box [1]; S-acylation, also specific for cysteines [2]; and N-terminal myristoylation [3]. In some cases synergistic action of two or more modifications and/or other factors such as polybasic amino acid sequences may also be important for the protein's interaction with the membrane.

Palmitoylation, the addition of the 16 carbon long acyl chain via a thioester linkage to target cysteine residues, occurs on a number of proteins, including α subunits of trimeric G proteins and Ras superfamily members [4, 5]. Unlike prenylation and myristoylation, palmitoylation is a reversible, dynamic process, with important implications for Gα protein regulation [6, 7]. Palmitoylation affects the interactions of Gα with Gβγ, receptors, effectors, and RGS proteins and the targeting of Gα to specific membrane sites [8–12]. In experiments using transfected cells, mutations involving cysteines susceptible to acylation in $G_s\alpha$, $G_q\alpha$, and $G_o\alpha$ led to impaired membrane localization [13, 14]. Activation of $G_s\alpha$, and presumably other G_s proteins, results in a significant increase in palmitate turnover [15–17]. It has been suggested that depalmitoylation may promote release of α subunits from the membrane [16, 18], but this has been contended by more recent studies [19].

The enzymatic machinery responsible for the reversible thioacylation is essentially uncharacterized. Protein palmitoyl thioesterase (PPT1) was originally implicated in the process, until it was found that, though physiologically important, the enzyme is localized to lysosomes [20] and cannot function in the G protein–mediated cascade. PPT1 is the product of the gene associated with infantile neuronal ceroid lipofuscinosis [21].

Recently, another 25 kDa acyl protein, thioesterase (APT1), has been identified, and it was demonstrated that it uses preferentially thioacylated proteins as substrates [22]. Interestingly, APT1 has been described earlier as a lysophospholipase [23, 24], although its activity on lysophospholipids is significantly lower than on palmitoyl-Gα [22]. In the murine lysophospholipase, mutagenesis experiments implicated Ser-119, Asp-174, and His-208 as active site residues [24, 25], suggesting that the protein is related to the ubiquitous superfamily of α/β hydrolases. Also, the protein is 34% identical in its amino acid sequence to a prokaryotic carboxylesterase from *Pseudomonas fluorescens*, the crystal structure of which revealed an α/β hydrolase fold [26].

Although thioesterases catalyze a plethora of physiologically important reactions, only four crystal structures have been reported to date. They include the *Vibrio harveyi* myristoyl-ACP-specific enzyme involved in bioluminescence [27], the 4-hydroxybenzoyl-CoA thioesterase from *Pseudomonas sp.* strain CBS-3 [28], the *E. coli* medium chain acyl-CoA thioesterase II [29], and the above mentioned PPT1, the only eukary-

Key words: α/β hydrolase; serine hydrolase; SAD; anomalous diffraction

otic thioesterase to be characterized structurally [30]. The *V. harveyi* and PPT1 proteins belong to the α/β hydrolase superfamily, which includes a large number of lipases, esterases, dehalogenases, and other, sometimes rare, enzymes [31]. In contrast, the other two prokaryotic thioesterases appear to be distant homologs, with similar, but notably different structures containing the so-called hot-dog domain motif.

In order to gain a better understanding of structure-function relationships in APT1, we solved the structure of the human isoform using a single-wavelength data set from a crystal containing Br^- ions. As expected, the protein show a tertiary fold of an α/β hydrolase, with the catalytic site made up of Ser-114, His-203, and Asp-169. Interestingly, the dimer observed in the unit cell is reminiscent of that described for the *P. fluorescens* carboxylesterase, although the physiological implications are not clear.

Results and Discussion

Structure Solution

Since the protein was overexpressed successfully in *E. coli*, we originally intended to use the MAD (multiwavelength anomalous dispersion) method. Protein samples containing SeMet were prepared in the usual way. However, no crystals were obtained from these samples, in contrast to wild-type protein. This is probably due to a relatively high methionine content of APT1 (nine methionine residues per molecule), and significant changes in the protein's solubility upon the introduction of SeMet. We have therefore turned to an alternative method, proposed recently by one of us [32], in which halide ions are introduced as anomalous scatterers in the cryoprotectant during a short soak. This technique, which obviates a lengthy and expensive process of producing Se-labeled protein, has been hitherto tested in several case studies using crystals with known structures and was used to solve a new protein of $\sim$300 residues with the use of 1M KI [32]. However, in the reported applications of the new method, a typical MAD protocol was followed, with several data sets (usually three) collected around the absorption edge. In the present study, strong anomalous signal observed at the high-energy remote wavelength prompted us to attempt phasing using a single data set. The programs SnB [33], SHARP [34], and DM from the CCP4 suite [35] were used to obtain an interpretable electron density map. Subsequently, wARP [36] was used to initiate model building with a complete data set to 1.8 Å resolution. The phasing was then extended to a partial set at 1.5 Å resolution (see Experimental Procedures). Figures 1a–1d show examples of electron density obtained using this phasing protocol. The atomic model was refined against a data set approaching 1.5 Å resolution. A difference anomalous Fourier map allowed for localization of 40 Br^- ions at the surface of the protein (Figure 1e).

Quality of the Model

The protein used in this study contains a 7 residue long N-terminal cloning artifact, followed by the sequence of hAPT1 starting at the methionine 6 (GenBank accession number C31610). This was chosen because the Kozak sequence is much more favorable than for the first methionine (see Experimental Procedures). The numbering in this report refers to the sequence starting at the new site.

The model consists of two independently refined protein molecules denoted A and B, 40 Br^- ions, and 465 water molecules. No noncrystallographic restraints were deemed necessary owing to high quality and good resolution of the data. The quality of the model was assessed by PROCHECK and shows 89% of the residues in most favored ϕ/ψ regions and no outliers except Ser-114 ($\phi = 53$, $\psi = -123$), which is located at the apex of the nucleophilic elbow and has the typical ϵ secondary conformation [37]. In each of the two 225 residue long polypeptide chains in the asymmetric unit, the electron density is continuous, with the exception of the first two amino acids of the of 7 residue long N-terminal cloning artifact and the C-terminal Asp-225. The loop including residues 153–158 in molecule A, as well as the one encompassing 80–84 in molecule B, are not as well defined as the remainder of the structure, an indication of localized flexibility in hAPT1. Final difference electron density map suggests alternative conformations for a total of 18 side chains in the two molecules, but at this stage static disorder was not modeled yet.

HAPT Is a Canonical α/β Hydrolase

The human APT is a canonical α/β hydrolase with a classical catalytic triad (see below) and with pronounced structural similarity to a carboxylesterase from *Pseudomonas fluorescens* (CPf) [26] (Figure 2). This observation is in concert with the mutagenesis studies of Wang et al. [25], which suggested that in the mouse enzyme, Ser-119, Asp-174, and His-208 are essential for catalysis, consistent with the existence of a catalytic trypsin-like triad and characteristic of α/β hydrolases. The α/β hydrolases are ubiquitous enzymes, which include neutral lipases, platelet-activating factor acetylhydrolase, esterases, dehalogenases, bromo-peroxidase, thioesterases, and others [31]. They share a common architecture of a central, predominantly parallel β sheet and connecting loops, which typically contain several helices. The loops on the carboxyl edge of the central β sheet in α/β hydrolases are typically more elaborate, and contain insertions of varying lengths and nature. These insertions often confer substrate specificity on the hydrolase (as is the case, for example, in brefeldin A esterase [38]) or are responsible for conformational changes during adsorption of the interfacial enzymes to the lipid phase [39].

The human APT1 is somewhat smaller and lacks the first β strand of the canonical fold. It also lacks a typical insertion after strand β6, but, like CPf, contains a long loop connecting strand β-4 with helix αB. This insertion is made up of four short antiparallel β strands (S1–S4), which form a small, irregular sheet. We will henceforth refer to this feature as the β4 loop (Figure 2c).

Least-squares comparison of the CPf and APT1 coordinates reveals that in spite of significant overall similarity, there are localized conformational differences between the two proteins (Figure 3). The mean difference calculated for the Cα atoms, taking into account several minor deletions and insertions, is 1.34 Å over 216 homologous residues. The key difference is in the conformation of the above-mentioned β4 loop, which folds closer toward the active site in hAPT1. As a result, Pro-75 located at the apex of the turn between strands S3 and S4 in the β4 loop assumes a position 13.9 Å away from the active site Ser-114, in contrast to Pro-75 in CPf, which is much further (17.7 Å) from Ser-114 (distances are calculated between Cα atoms). Structural elements close to β4 are also affected by the conformational change to a varying extent. As we will show, the conformational change of the β4 loop has important implications for the dimerization mode of the enzyme and for the stereochemistry of the active site.

Other conformational differences are localized in the follow-

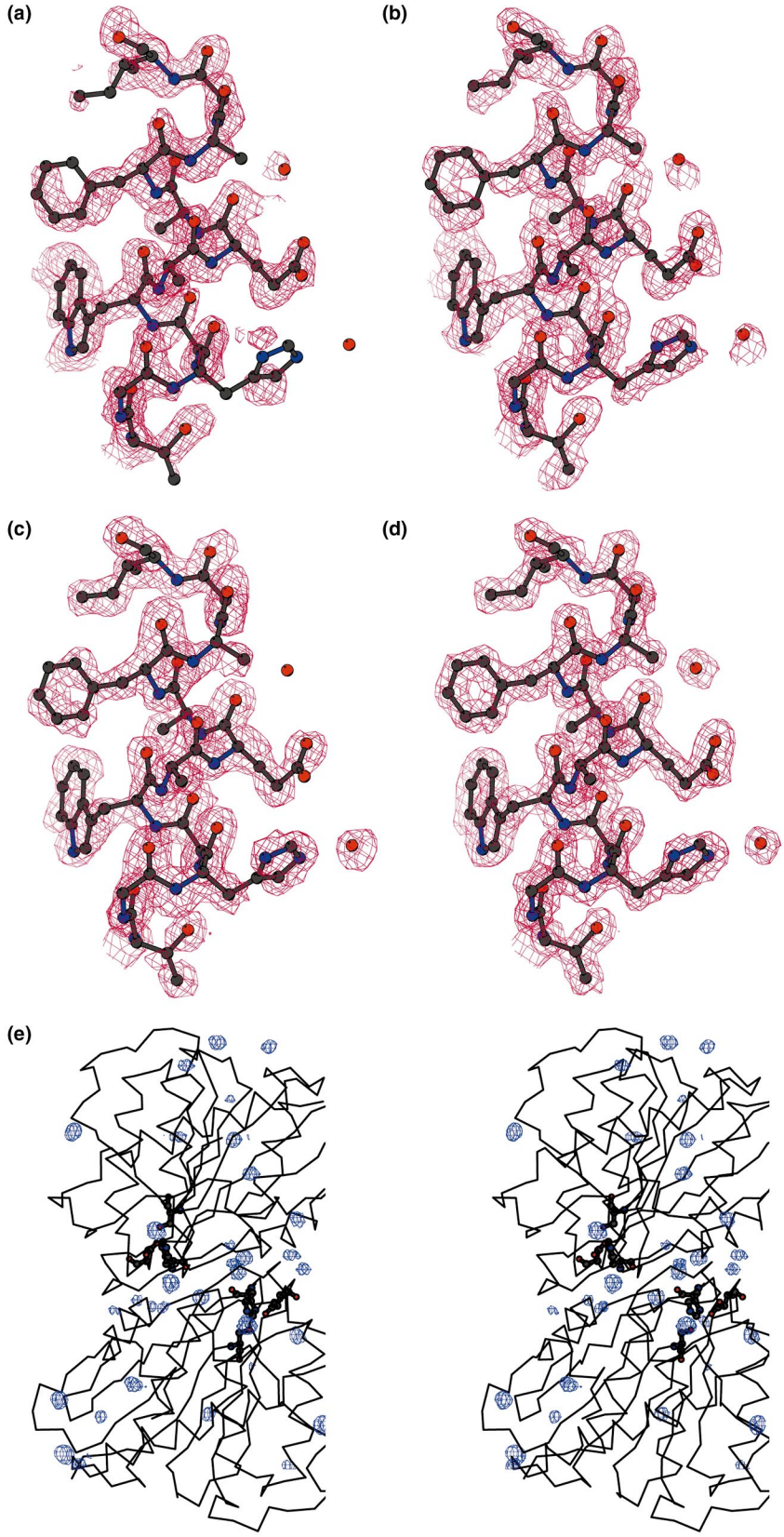

Figure 1. Phasing of Human APT1 from Solvent Bromide Ions

Representative $2F_o$-F_c electron densities during the course of structure solution and refinement contoured at 1σ: (a) after DM; (b) after first wARP at 1.8 Å resolution; (c) after wARP at 1.5 Å resolution; and (d) refined model at 1.5 Å resolution. (e) Location of the Br^- ions bound at the surface of hAPT1; hAPT1 dimer is shown by Cα trace with the catalytic triads shown in full. The difference anomalous Fourier map, which reveals the locations of the Br^- ions, is based on a refined protein model and is contoured at a 4 σ level.

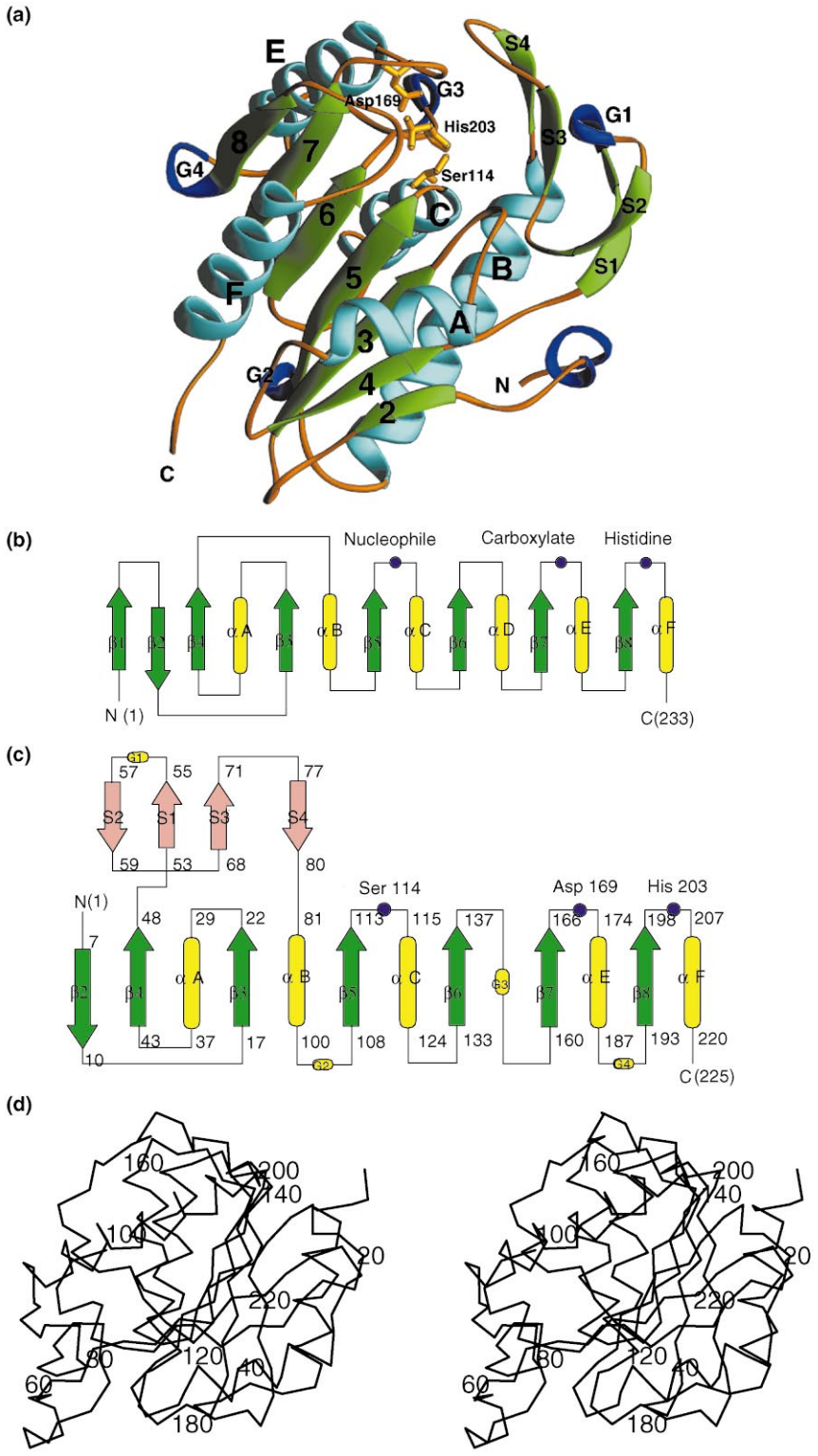

Figure 2. Structure of Human APT1

(a) Ribbon diagram presenting the secondary structure elements. Seven β strands (green arrows) are numbered sequentially from 2 to 8 (the canonical strand 1 is missing). Four short β irregular strands are denoted S1–S4. Five α helices (in blue) are labeled from A to F according to the structure of a canonical α/β hydrolase (see Figure 2). Four short helical segments (in dark blue) are labeled from G1 to G4. Catalytic residues Ser-114, Asp-169, and His-210 are shown as golden ball and stick models.

(b) Topology diagram of a canonical α/β hydrolase.

(c) Topology of human APT1. Eight strands (green arrows) labeled as β1–β8 and six helices (yellow rods) labeled as αA–αF constitute the canonical α/β fold. Human APT1 lacks the first β strand (β1), the fourth α helix (αD) is replaced by a short helical segment, G3, and there are additionally four short β strands (S1–S4). Blue circles show the catalytic residues in hAPT1 and in the canonical α/β hydrolase. The residue numbers at the N and C termini of hAPT1 correspond to the construct used in this study (see Experimental Procedures for details).

(d) Stereo Cα trace of the protein molecule. Every twentieth residue is labeled.

ing regions: residues 3–14, the first β strand, with maximum difference of 3.6 Å between corresponding Cα atoms; residues 69–78, which constitute a part of the β4 loop in close proximity of the active site (maximum difference of 6.9 Å); the loop 142–159, preceding strand 7, with maximum difference of 5.8 Å; and loop 187–191, preceding strand 8, with maximum difference of 6.0 Å.

Both proteins are representatives of a family found throughout the living world. A BLAST search based on the hAPT1 sequence revealed at least 34 unique homologs, found in such

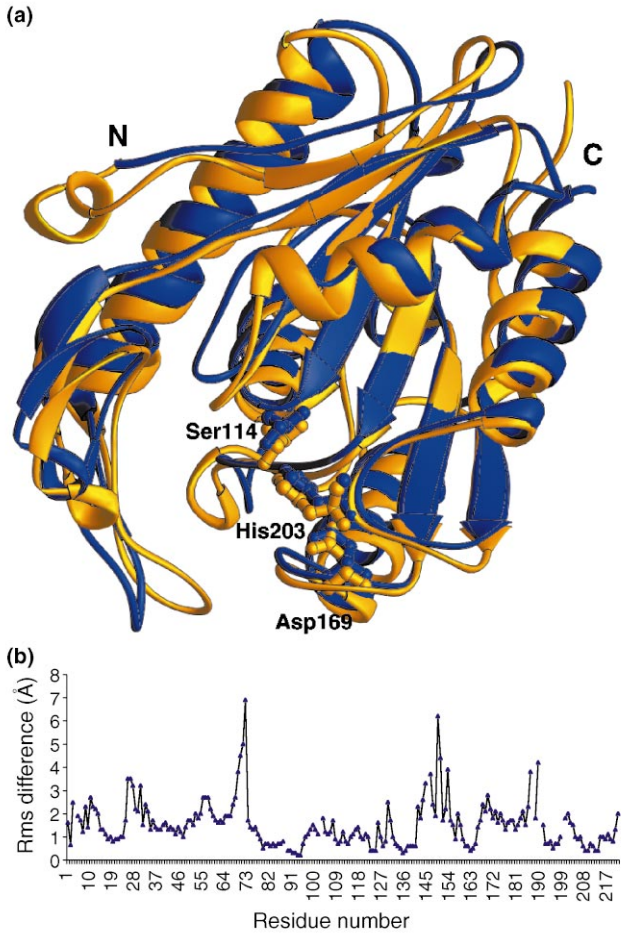

Figure 3. Comparison of the Structures of hAPT1 and CPf

(a) Ribbon presentation of the superposition of Cα atoms of carboxyl esterase (blue) onto the structure of hAPT1 (gold). Labeled active site residues are shown by ball and stick models.

(b) Difference distance plot of the corresponding Cα atoms.

diverse species as human, *Schistosoma mansoni*, *Drosophila melanogaster*, *Saccharomyces cerevisiae*, *Caenorhabditis elegans*, *Arabidopsis thaliana*, and *Mycobacterium leprea* and others. Figure 4 shows sequence alignment of several enzymes with predicted structural features based on the hAPT1 structure.

The Noncrystallographic Dimer

With few exceptions, the α/β hydrolases are monomeric enzymes. The homodimeric *P. fluorescens* carboxylesterase has been reported to be one such exception, and we anticipated that the noncrystallographic dimer found in the hAPT1 crystal would correspond to that described for CPf. Unexpectedly, we find that in the hAPT1 dimer, the association of monomers is different from CPf, even though in both cases the active sites of the enzymes are brought to close proximity.

The CPf homodimer is held together by close symmetric interactions of the β4 loops as well as interactions between two loops that follow strands β7 and β8, so that the β7 loop interacts with the β8 loop of the neighboring molecule. The two close contacts leave space adequate to allow sufficient access for monomeric substrate to reach the active site. By contrast, in the hAPT1 dimer the mutual disposition of the molecules is altered, although the same loops make up the interface (Figure 5). The β4 loop in hAPT1 shifts away from the interface, and the molecules are rearranged through rotation and translation so that the β4 loops interact side-to-side through the S2 strands only. The β7 and β8 loops are shifted so that the β8 loops only interacts with its counterpart in the second molecule, while the β7 loop forms a novel interaction with residues on the αA helix. This new contact, together with additional involvement of several residues from the N terminus, significantly extends the buried surface, as compared to the carboxylesterase, to a total of 2,350 Å^2, or 11.5% of the combined surfaces of the two monomers. The corresponding values for carboxylesterase are 1,306 Å^2 and 6.6%. More significantly, the access to the active site is now severely restricted, and it is difficult to see how a substrate might reach the nucleophilic serine without the concomitant dissociation of the dimer. We note, that the dimer interface is not contiguous, but it encapsulates a fairly large cavity of ~200 Å^3 filled with at least 10 ordered water molecules; this is likely to increase the dissociation constant for the hAPT1 homodimer in comparison to other dimeric proteins exhibiting interfaces of comparable surface.

A pressing question is whether the homodimer observed in the crystal is representative of the species found in solution. Gel filtration experiments (data not shown) indicate that in the

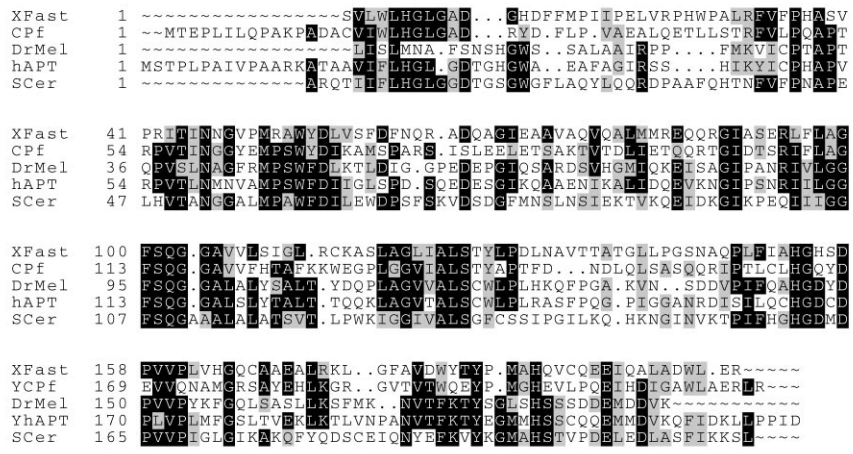

Figure 4. Sequence Alignment of the ACP1 Family of Enzymes

Structure-guided sequence alignment of representative enzymes belonging to the APT/carboxylesterase family of α/β hydrolases: Xfast: *Xylella fastidiosa*, section 135 of 229 of the complete genome, code AE003989, 35% identity with hAPT1; Cpf: *P. fluorescens* carboxylesterase, code S79600, 34% identity with hAPT1; hAPT1: human acyl protein thioesterase 1; DrMel: *Drosophila melanogaster*, code AE003544, 51% identities with hAPT1; SCer: *Saccharomyces cerevisiae* DNA from chromosome XII right arm, code X89514, 36% identity with hAPT1.

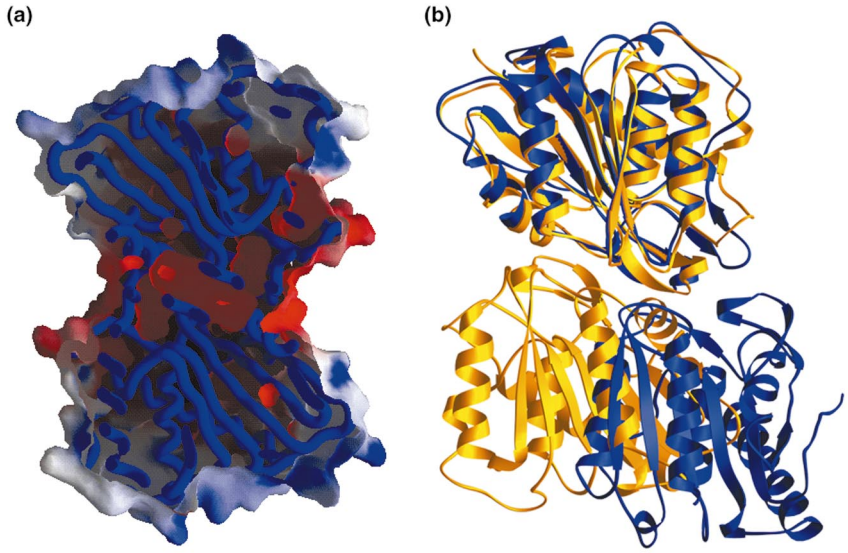

Figure 5. The Noncrystallographic hAPT1 Dimer

(a) Cutaway view of the electrostatic potential surface of the noncrystallographic dimer; the cavity located at the dimer interface is shown in red, and the blue tube represents the backbone. Positively charged regions are blue and negative regions are red.

(b) A comparison of the noncrystallographic dimer of hAPT1 and CPf dimer. A subunit of CPf (blue ribbons) is superimposed onto molecule A in hAPT1 dimer (gold ribbons).

presence of 200 mM NaCl and 5mM β-mercaptoethanol, there is equilibrium of monomeric and dimeric species of hAPT1, the latter most likely corresponding to the non-crystallographic dimer. It is not clear at this point if the observed dimerization mode is physiologically relevant. Further studies, underway in our laboratories, will address this issue.

The Architecture of the Active Site

All α/β hydrolases contain the active site in the same topological location, with the nucleophilic residue residing on a sharp turn between the central β strand and a buried α helix [40]. This residue, typically a serine, although aspartates and cysteines have also been observed, is in a strained secondary conformation known as the ϵ-conformation [37]. In hAPT1, Ser-114 is the nucleophile. It is located in the proximity of His-203, which in turn donates an H-bond (2.9 Å) from Nδ1 to Oδ1 of Asp-196. The Oδ2 atom of Asp-196 is firmly anchored via two strong H-bonds donated by the main chain amides of Leu-171 and Leu-172, ensuring conformational rigidity of the Asp-His pair. The mutual disposition of all the amino acids in this ensemble is typical for chymotrypsin-like serine hydrolases.

The details of the active sites in the A and B molecules vary slightly, probably due to different crystal packing. In molecule A, the position of Ser-114 is such that, in spite of spatial proximity, no H-bond with Nϵ2 of His-206 is possible. When we compared the stereochemistry of this site to that of CPf, we find that in hAPT1 the catalytic Asp-His pair is shifted in concert with respect to the core of the structure, including the catalytic Ser-144. The site typically occupied by the hydroxyl is taken by a well-ordered water molecule (Wat-55) (Figure 6a). This distortion from the typical ground state stereochemistry of serine hydrolases is less pronounced in molecule B, where both the hydroxyl of Ser-144 and Wat-55 appear to be within H-bonding distance of His 206. It is possible, that the somewhat unusual geometry of the active site in hAPT1 is the result of crystal packing, particularly the tight interaction of the molecules in the noncrystallographic dimer. It is also possible that the perturbations in the active site are the result, at least in part, of the Br^- ions bound in its proximity, and particularly of the ion occupying the oxyanion hole. We intend to verify this point by refining a crystal structure using data from a Br^- free crystal. Whatever the causes of the relative changes observed in the active site, the flexibility of the molecule may have important implications for catalysis. Serine-dependent hydrolases catalyze a two-step reaction involving acylation and deacylation, each proceeding via a tetrahedral transition state. In the ground state, the enzyme is thought be active due to the interaction of the dyad Asp-His, which activates the nucleophilic serine by providing a proton sink. In the acyl-enzyme intermediate, the acylated serine shifts away from the catalytic histidine, providing room for a water molecule which, again through an interaction with the Asp-His dyad, is rendered nucleophilic and attacks the scissile ester bond on the serine. This water molecule is rarely observed in crystal structures, because acyl-enzyme intermediates are intrinsically unstable. However, it has been seen in the structures of γ-chymotrypsin and trypsin [41, 42].

The mechanism of serine-dependent hydrolases relies, to a degree, on the flexibility in the active site region to allow for the relative shift of the Asp-His dyad relative to the serine. The structure of hAPT1 appears to be closer to that expected at the deacylation step, including the presence of a water molecule hydrogen bonded to the Nϵ2 of His-206. This water is not seen, to our knowledge, in other structures of ground state serine hydrolases.

The transient oxyanions that occur during acylation and deacylation steps are stabilized in the course of the reaction in a positively charged oxyanion hole, a feature which contributes significantly to the catalytic efficiency of serine hydrolases. Prior studies of enzymes related to hAPT1, particularly neutral lipases [43], allow one to infer the location of the oxyanion hole, which appears to be formed by the main chain amides of Leu-25 and Gln-115. It is interesting to note that the most tightly bound Br^- ions (as indicated by the associated B factors) are found in the oxyanion holes of the two independent molecules in the asymmetric unit.

The putative acyl binding pocket is lined with a number of hydrophobic residues (Trp-140, Leu-68, Leu-73, and Phe-176). These residues correspond closely to the pocket identified in CPf, even though the putative substrate in the latter enzyme

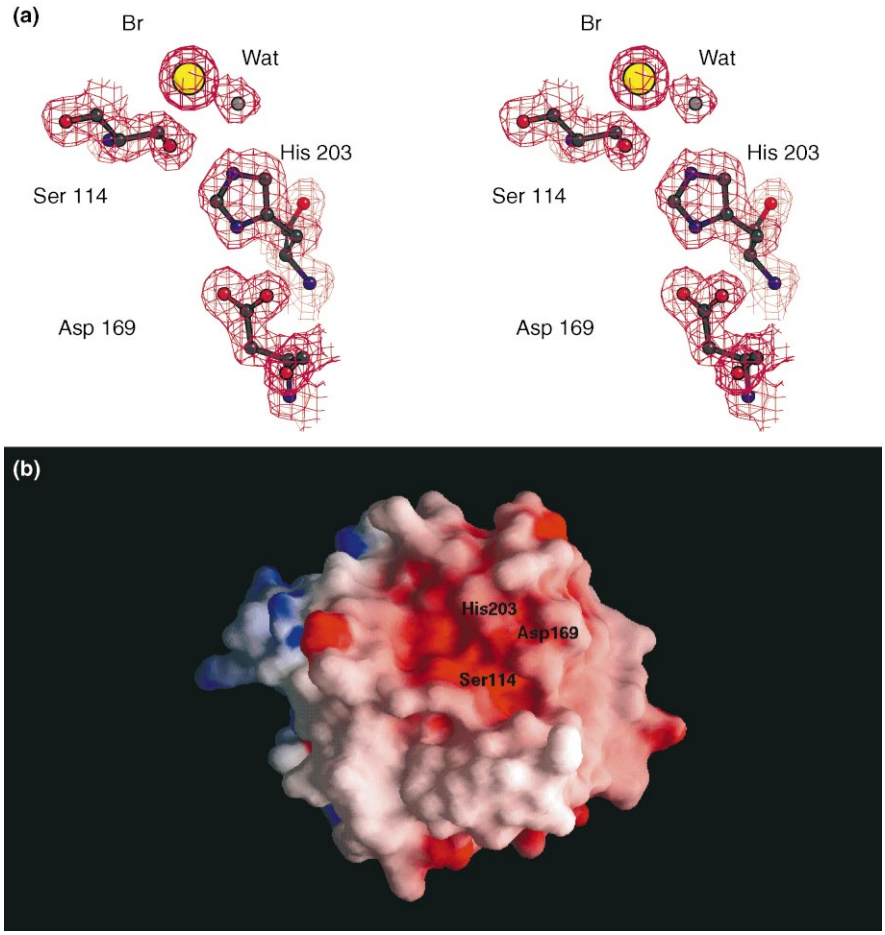

Figure 6. Active Site of hAPT1

(a) Electron density for the active site region of the refined model contoured at 1 σ level. Side chains of Ser-114, Asp-169, and His-203 are presented as ball and stick models, Wat-55 as a gray sphere, and Br^- ion as a yellow sphere.

(b) A view of the monomer obtained by 90° rotation around a horizontal axis. Labels show location of the active site residues Ser-114, Asp-169, and His-210 at the dimer interface.

is significantly smaller. Further studies will be needed to address the nature of specificity determinants in the two enzymes.

The electrostatic potential surface, calculated using GRASP, reveals that the vicinity of the active site carries a distinct negative charge (Figure 6b). Detailed analysis shows that with the exception of Asp-27, all residues in that region are neutral, and the negative charge is largely conferred by main chain carbonyls. The negative potential surrounding the active site is a common feature among esterases and lipases and is typically thought to assist in the expulsion of the negatively charged reaction product; hAPT1 appears to conform to that paradigm.

Table 1. X-Ray Experimental Data

	Basic Data Set	Extended Data Set
Resolution (Å)	1.8	1.48
Number of reflections		
Total	129,461	163,216
Unique	35,227	50,736
Redundancy	3.7	3.2
Completeness (%)	99.9 (99.8)[a]	80.0 (27.1)
R_{sym} (%)[b]	4.8 (12.3)	5.2 (34.3)
I/σ ratio	20.3 (5.8)	17.0 (2.5)

[a] The numbers in parentheses describe the relevant value for the last resolution shell.

[b] R_{sym} $\Sigma|I_i - <I>|/\Sigma I$ where I_i is the intensity of the ith observation and $<I>$ is the mean intensity of the reflections.

Comparison with Other Thioesterases

To date, four structures of thioesterases have been published. Two of those, the 4-hydroxybenzoyl CoA thioesterase from *Pseudomonas* [28] and medium-length chain thioesterase II from *E. coli*, appear to be distantly related and share a similar folding architecture, although the *E. coli* protein is larger and contains two repeats of the same fold, with only one being catalytically active. It has been proposed, based on structural considerations as well as mutagenesis, that an aspartate residue acts as the catalytic amino acid by activating a water molecule for a nucleophilic attack on the thioester carbon. By contrast, the *Vibrio harveyi* myristoyl acyl carrier protein (C14:ACP) thioesterase [27] and the recently determined palmitoyl protein thioesterase (PPT1) [30] are α/β hydrolases harboring classical catalytic triads of Ser, His, and Asp and are closely related to a plethora of oxyesterases and lipases (i.e., interfacially active acylglycerol esterases), which show similar molecular architectures. It is not clear why thioesterases show such structural diversity. It is noteworthy, however, that the α/β family of thioesterases known to date appear to act primarily on acylated proteins, while the Asp-dependent family members target CoA thioesters. The interactions of α/β thioesterases with the protein moieties of the substrates have not been elucidated, and the epitopes responsible for them are not known. On the other hand, acyl binding pockets are typically conspicuous, and in the case of PPT1 clearly visualized by the PPT1-palmitate complex.

Table 2. Bromide Ions Used for Initial Phasing of the Structure of hAPT1

Number	X	Y	Z	Relative Oc.	B factor
1	0.073153	0.235505	0.617810	1.45457	7.33631
2	0.329881	0.134384	0.873337	1.43614	7.92465
3	0.044658	0.496915	0.834845	1.30345	14.79730
4	0.774109	0.372586	0.002740	1.09472	12.72298
5	0.182389	0.555359	0.670043	1.31161	23.09031
6	0.388052	0.816253	0.864343	0.95836	16.55794
7	0.137981	0.179254	0.623225	0.90124	16.30678
8	0.324809	0.192553	0.809571	0.60372	4.40490
9	0.806411	0.341808	0.445394	0.88136	14.05303
10	0.453537	0.164221	0.375549	0.55010	4.56460
11	0.501695	0.028265	0.138991	0.65495	10.26043
12	0.441275	0.437285	0.508077	0.40410	4.07911
13	0.574134	0.207333	0.497000	0.69068	13.09224
14	0.730955	0.123371	0.628061	0.47654	7.14637
15	0.894231	0.072086	0.719620	0.90036	31.70239
16	0.379532	0.432474	0.949129	0.31567	1.00000
17	0.529769	0.331896	0.501163	0.62532	14.56022
18	0.224882	0.297486	0.053001	0.41933	8.54289
19	0.395525	0.336649	0.302980	0.46323	16.42011
20	0.458053	0.039489	0.419730	0.38986	5.66594
21	0.319697	0.247954	0.221739	0.48968	16.32407
22	0.607640	0.209658	0.773284	0.31314	4.30829

Biological Implications

The study reported in this paper impacts on two disparate areas of structural biology. First, the ease in solving the 58 kDa structure (the asymmetric unit) by using a single data set collected from a wild-type protein crystal containing bromide salt suggests wider applicability of these methods. It is widely accepted that in the near future, structural biology must significantly enhance its throughput to cope, at least to some degree, with the dramatic growth of genomic data. To date, the most efficient method of crystal structure solution is MAD (multiwavelength anomalous dispersion method), with SeMet-substituted protein crystals. Although the method enjoys well-deserved popularity, it relies on the availability of SeMet-labeled protein samples, crystallizability of these samples, and calls for at least three data sets collected at the absorption peak, inflection point, and high-energy remote wavelengths. The approach used in our work obviates the need to overexpress Se-labeled protein and significantly reduces the time used at the synchrotron beamline.

Second, a novel protein involved in G protein–mediated signal transduction has been characterized at high resolution. Like many other oxy- and thioesterases, the human APT1 is a canonical α/β hydrolase containing a classical serine triad made up of Ser-114, Asp-169, and His-203. The atomic model reveals profound similarities with the *Pseudomonas fluorescens* carboxylesterase, although there are significant conformational differences between the two, involving primarily the β4 loop. The crystal structure shows that the enzyme is a homodimer, related in general terms to the *P. fluorescens* enzyme, but one in which, unexpectedly, the active site is occluded from bulk solvent. This may suggest a novel regulatory mechanism involving dissociation of the homodimer probably induced by substrate binding, although further studies are required to probe this hypothesis.

Table 3. Refinement Details

Resolution used in final refinement (Å)	20.0–1.5
R_{cryst}/R_{free} (%)[a]	18.6/23.7
Rms deviations from target bond lengths (Å)/bond angles (°)	0.018/1.45
Rms deviations from <B> (Å^2) overall	2.23
Average B factors (Å^2)	
Main chain atoms	13.5
Side chain atoms	16.3
Waters	28.2

[a] $R_{cryst} = \Sigma||F_o| - |F_c||/\Sigma|F_o|$, where F_c is calculated structure factor.

Experimental Procedures

Expression of Human APT-1 in *E. coli*

To amplify the entire coding region of hAPT1, oligonucleotide primers (EcoRI site [sense], 5'-GGCTCGAATTCATGTCAACCCCGCTG-3'; XhoI site [antisense], 5'-GGCTCCTCGAGTCTACTACAATGATGCTGGTG-3' were used in a polymerase chain reaction using Human Testis Marathon-Ready c-DNA (Clontech) as a template. The amplified product was digested with EcoRI and XhoI and ligated into the expression vector pHis Parallel I [44]. Open reading frame and polymerase fidelity was verified by dideoxynucleotide sequencing. The resulting plasmid was transformed into *E. coli* BL21(DE3) (Novagen). The cells were grown at 37°C in 1 l of LB broth containing 50 μg/ml ampicillin to an OD_{600} of 0.6–0.8, and expression was initiated by the addition of IPTG to a final concentration of 1 mM. The culture was grown for an additional 4 hr at 37°C. The cells were harvested by centrifugation at 6500 $\times$ g for 15 min at 4°C. The pellet was resuspended in ice-cold H buffer (5 mL/g) (150 mM NaCl, 50 mM Tris-HCl [pH 8.0]) and sonicated on ice using ten 10 s bursts with a 10 s cooling period between each burst. The cellular debris was pelleted by centrifugation at 12,000 $\times$ g for 30 min at 4°C, and supernatant was used for further purification of hAPT1.

Purification of hAPT1

Purification of His-tagged hAPT1 was carried out by established methods [44] with slight modifications. The supernatant was incubated with 5 ml of preequilibrated (H buffer) Ni^{2+}-NTA agarose for 2 hr at 4°C to bind the His_6-tagged hAPT1, and the resin was washed with 2 l of H buffer at 4°C. The bound protein was eluted with 20 ml of H buffer containing 250 mM imidazole (pH 8.0). The His_6-tag was cleaved with 800 units of His_6-tagged rTEV protease (Life Technologies) for 36 hr at 15°C in a 15 ml Slide-a-Lyser cassette (Pierce) during dialysis against 4 l of H buffer to remove imidazole and the cut His_6-tag sequence. The dialyzed solution was incubated with 5 ml of Ni^{2+}-NTA agarose for 2 hr at 4°C to remove both uncut protein and rTEV protease. DTT, EDTA, and glycerol were added to a final concentration of 5 mM, 1 mM, and 5%, respectively, and protein was concentrated to 15–20 mg/mL by using an Amicon 8050 ultrafiltration unit with an YM 10 membrane (10,000 MWCO) (Millipore) in a cold room.

The amino-terminal sequence of the purified protein starts with seven amino acids from the tag sequence, i.e., a cloning artifact, GAMDPEF, followed by the sequence of hAPT1. The latter starts with MSTPLP, a more favorable start site found five amino acids downstream from the original start site shown in the GenBank entry C31610. The numbering of amino acids in this report starts with the methionine in the MSTPLP sequence.

Crystallization

Recombinant hAPT1 was dialyzed against 20 mM tris-HCl buffer, pH 8.0 with addition of 30 mM NaCl and 5 mM dithiotreitol (DTT). Dialyzed protein was concentrated to 8 mg/ml and crystallized by vapor diffusion against reservoir containing 28%–32% of saturation ammonium sulfate in 100 mM Na-acetate buffer (pH 5.0) with addition of 1%–2% v/v 2,4-dimethyl pentanediol (MPD). Clusters of crystals appear within a week or two; however, single crystals with maximal dimensions 0.2 $\times$ 0.1 $\times$ 0.1 mm grow over three weeks to a month.

Structure Solution and Model Refinement

A single crystal of wild-type protein was flash frozen using artificial mother liquor solution containing 42% of saturation ammonium sulfate in 100 mM Na-acetate buffer with addition of 20% v/v glycerol and 1 M NaBr and 20 s soaking time. Data were collected at beamline X9B of the National Synchrotron Light Source (Brookhaven National Laboratory) using a Quantum4 ADSC CCD area detector. The wavelength, 0.91674 Å, was set to correspond to 50 eV above the K-edge, i.e., remote high energy. The crystal was a thin plate and the long axis was nearly perpendicular to the rotation axis. To avoid excessive overlap, the distance was set to obtain a full data

set to 1.8 Å resolution, even though crystals diffracted to 1.2 Å. A total of 360 frames, each corresponding to 0.5° rotation, was collected with 45 s exposure time. The unit cell was identified with DENZO as $P2_1$, a = 39.5 Å, b = 127.9 Å, c = 39.7 Å, β = 102.8° (V_m = 1.96 Å³/Da). Data were reduced with HKL2000 [45]. Details are shown in Table 1. Anomalous differences from the data set processed to 1.8 Å resolution were used to identify a subset of Br^- ions using SnB [33]. A number of solutions with low R_{min} suggested that the problem was solvable. One of the solutions was chosen as a starting point for phase calculation using SHARP [34]. The substructure input to SHARP consisted of seven sites. Using residual difference maps in SHARP, additional sites were identified and iteratively input into phasing until 22 sites were obtained (Table 2). Upon visual inspection, 16 exhibited clear noncrystallographic symmetry, which conferred credibility on the solution. Using the single data set to 1.8 Å resolution, the substructure was used to compute phases with an overall FOM of 0.40; the phases were modified in DM using default settings, and FOM was increased to 0.85. The resulting electron density map was clearly interpretable. In an effort to further improve the map, we used free atom refinement procedure and automatic chain tracing as implemented in wARP [36]. The outcome was most encouraging, and we decided to take one more step before manual model building. We reprocessed all data to include the reflections in the corners of the square detectors out to 1.5 Å resolution. Although the data in the outermost shell are incomplete, over 15,000 additional reflections (~30% of the 1.8 Å set) were subsequently found to be very helpful during refinement. Using the new data set, we re-ran wARP, this time allowing for automatic model building from the input sequence. As a result, 347 residues (57 had side chains corresponding to the original amino acid sequence) out of 464 for the both molecules in the asymmetric unit were fitted automatically; in other areas the density was improved sufficiently to allow for effortless model building using O [49] (N.B., after the model was built, we experimented with different sampling procedures for wARP and found that up to 130 amino acid residues per molecule with complete side chains could have been built automatically). Upon completion of model building, the structure was refined using a maximum likelihood target in REFMAC [35], with automatic recognition of water molecules in wARP. The sites occupied by Br^- ions were verified at the end of the refinement using a ΔF_{anom} Fourier with model phases shifted by 90°. Forty peaks above 3.5 σ were found, and all were included in the refinement as Br^- ions, although at this point reliable evaluation of their true occupancy factors is not possible. Details of phasing and refinement are provided in Table 3.

Miscellaneous

Figures were prepared using BOBSCRIPT [46], Ribbons [47], GRASP [48], and O [49]. Least square fit was performed with Shelx [50].

Acknowledgments

The study was funded by the National Institutes of Health, in part by grant HL48807. We thank Sarah M. Garrard for size exclusion chromatography and Dr. Jia Li for help with the figures.

Received: August 3, 2000
Revised: September 20, 2000
Accepted: September 22, 2000

References

1. Fu, H.W., and Casey, P.J. (1999). Enzymology and biology of CaaX protein prenylation. Recent Prog. Horm. Res. *54*, 315–342.
2. Deschenes, R.J., Resh, M.D., and Broach, J.R. (1990). Acylation and prenylation of proteins. Curr. Opin. Cell Biol. *2*, 1108–1113.
3. Taniguchi, H. (1999). Protein myristoylation in protein-lipid and protein-protein interactions. Biophys. Chem. *82*, 129–137.
4. Dunphy, J.T., and Linder, M.E. (1998). Signalling functions of protein palmitoylation. Biochim. Biophys. Acta *1436*, 245–261.
5. Linder, M.E., Middleton, P., Hepler, J.R., Taussig, R., Gilman, A.G., and Mumby, S.M. (1993). Lipid modifications of G proteins: alpha subunits are palmitoylated. Proc. Natl. Acad. Sci. USA *90*, 3675–3679.
6. James, G., and Olson, E.N. (1990). Fatty acylated proteins as components of intracellular signaling pathways. Biochemistry *29*, 2623–2634.
7. Morello, J.P., and Bouvier, M. (1996). Palmitoylation: a post-translational modification that regulates signalling from G-protein coupled receptors. Biochem. Cell Biol. *74*, 449–457.
8. Iiri, T., Backlund, P.S., Jr., Jones, T.L., Wedegaertner, P.B., and Bourne, H.R. (1996). Reciprocal regulation of Gs alpha by palmitate and the beta gamma subunit. Proc. Natl. Acad. Sci. USA *93*, 14592–14597.
9. Ponimaskin, E., Harteneck, C., Schultz, G., and Schmidt, M.F. (1998). A cysteine-11 to serine mutant of G alpha12 impairs activation through the thrombin receptor. FEBS Lett. *429*, 370–374.
10. Jones, T.L., and Gutkind, J.S. (1998). Galpha12 requires acylation for its transforming activity. Biochemistry *37*, 3196–3202.
11. Tu, Y., Wang, J., and Ross, E.M. (1997). Inhibition of brain Gz GAP and other RGS proteins by palmitoylation of G protein alpha subunits. Science *278*, 1132–1135.
12. Bhattacharyya, R., and Wedegaertner, P.B. (2000). Galpha 13 requires palmitoylation for plasma membrane localization, Rho-dependent signaling, and promotion of p115-RhoGEF membrane binding. J. Biol. Chem. *275*, 14992–14999.
13. Wedegaertner, P.B., Chu, D.H., Wilson, P.T., Levis, M.J., and Bourne, H.R. (1993). Palmitoylation is required for signaling functions and membrane attachment of Gq alpha and Gs alpha. J. Biol. Chem. *268*, 25001–25008.
14. Grassie, M.A., McCallum, J.F., Guzzi, F., Magee, A.I., Milligan, G., and Parenti, M. (1994). The palmitoylation status of the G-protein G(o)1 alpha regulates its activity of interaction with the plasma membrane. Biochem. J. *302*, 913–920.
15. Mumby, S.M., Kleuss, C., and Gilman, A.G. (1994). Receptor regulation of G-protein palmitoylation. Proc. Natl. Acad. Sci. USA *91*, 2800–2804.
16. Wedegaertner, P.B., and Bourne, H.R. (1994). Activation and depalmitoylation of Gs alpha. Cell *77*, 1063–1070.
17. Degtyarev, M.Y., Spiegel, A.M., and Jones, T.L. (1993). Increased palmitoylation of the Gs protein alpha subunit after activation by the beta-adrenergic receptor or cholera toxin. J. Biol. Chem. *268*, 23769–23772.
18. Wedegaertner, P.B., Wilson, P.T., and Bourne, H.R. (1995). Lipid modifications of trimeric G proteins. J. Biol. Chem. *270*, 503–506.
19. Huang, C., Duncan, J.A., Gilman, A.G., and Mumby, S.M. (1999). Persistent membrane association of activated and depalmitoylated G protein alpha subunits. Proc. Natl. Acad. Sci. USA *96*, 412–417.
20. Verkruyse, L.A., and Hofmann, S.L. (1996). Lysosomal targeting of palmitoyl-protein thioesterase. J. Biol. Chem. *271*, 15831–15836.
21. Vesa, J., et al., and Peltonen, L. (1995). Mutations in the palmitoyl protein thioesterase gene causing infantile neuronal ceroid lipofuscinosis. Nature *376*, 584–587.
22. Duncan, J.A., and Gilman, A.G. (1998). A cytoplasmic acyl-protein thioesterase that removes palmitate from G protein alpha subunits and p21(RAS). J. Biol. Chem. *273*, 15830–15837.
23. Sugimoto, H., Hayashi, H., and Yamashita, S. (1996). Purification, cDNA cloning, and regulation of lysophospholipase from rat liver. J. Biol. Chem. *271*, 7705–7711.
24. Wang, A., Deems, R.A., and Dennis, E.A. (1997). Cloning, expression, and catalytic mechanism of murine lysophospholipase I. J. Biol. Chem. *272*, 12723–12729.
25. Wang, A., Loo, R., Chen, Z., and Dennis, E.A. (1997). Regiospecificity and catalytic triad of lysophospholipase I. J. Biol. Chem. *272*, 22030–22036.
26. Kim, K.K., et al., and Suh, S.W. (1997). Crystal structure of carboxylesterase from Pseudomonas fluorescens, an alpha/beta hydrolase with broad substrate specificity. Structure *5*, 1571–1584.
27. Lawson, D.M., et al., and Derewenda, Z.S. (1994). Structure of a myristoyl-ACP-specific thioesterase from Vibrio harveyi. Biochemistry *33*, 9382–9388.
28. Benning, M.M., Wesenberg, G., Liu, R., Taylor, K.L., Dunaway-Mariano, D., and Holden, H.M. (1998). The three-dimensional structure of 4-hydroxybenzoyl-CoA thioesterase from Pseudomonas sp. Strain CBS-3. J. Biol. Chem. *273*, 33572–33579.
29. Li, J., Derewenda, U., Dauter, Z., Smith, S., and Derewenda, Z.S. (2000). Crystal structure of the *Escherichia coli* thioesterase II, a homolog of the human Nef binding enzyme. Nat. Struct. Biol. *7*, 555–559.
30. Bellizzi, J.J., 3rd, et al., and Clardy, J. (2000). The crystal structure of palmitoyl protein thioesterase 1 and the molecular basis of infantile neuronal ceroid lipofuscinosis. Proc. Natl. Acad. Sci. USA *97*, 4573–4578.
31. Heikinheimo, P., Goldman, A., Jeffries, C., and Ollis, D.L. (1999). Of barn owls and bankers: a lush variety of alpha/beta hydrolases. Structure *7*, R141–R146.
32. Dauter, Z., Dauter, M., and Rajashankar, K.R. (2000). Novel approach to phasing proteins: derivatization by short cryo-soaking with halides. Acta Crystallogr. D Biol. Crystallogr. *56*, 232–237.

33. Weeks, C.M., and Miller, R. (1999). The design and implementation of SnB v2.0. J. Appl.Crystallogr. *32*, 120–124.
34. de la Fortelle, E., and Bricogne, G. (1997). Maximum-likelihood heavy atom parameter refinement for multiple isomorphous replacement and multiwavelength anomalous diffraction methods. Methods Enzymol. *276*, 472–494.
35. Collaborative Computing Project Number 4 (1994). The CCP4 suite: programs for protein crystallography. Acta Cryst. *D50*, 760–763.
36. Perrakis, A., Morris, R., and Lamzin, V.S. (1999). Automated protein model building combined with iterative structure refinement. Nat. Struct. Biol. *6*, 458–463.
37. Derewenda, Z.S., and Derewenda, U. (1991). Relationships among serine hydrolases: evidence for a common structural motif in triacylglycerol lipases and esterases. Biochem. Cell Biol. *69*, 842–851.
38. Wei, Y., et al., and Derewenda, Z.S. (1999). Crystal structure of brefeldin A esterase, a bacterial homolog of the mammalian hormone-sensitive lipase. Nat. Struct. Biol. *6*, 340–345.
39. Van Tilbeurgh, H., Egloff, M.-P., Martinez, C., Rygani, N., Verger, R., and Cambillau, C. (1993). Interfacial activation of the lipase-prolipase complex by mixed micelles revealed by X-ray crystallography. Nature *362*, 814–820.
40. Ollis, D.L., et al., and Goldman, A. (1992). The α/β hydrolase fold. Protein Eng. *5*, 597–611.
41. Dixon, M.M., and Matthews, B.W. (1989). Is gamma-chymotrypsin a tetrapeptide acyl-enzyme adduct of alpha-chymotrypsin? Biochemistry *28*, 7033–7038.
42. Singer, P.T., Smalas, A., Carty, R.P., Mangel, W.F., and Sweet, R.M. (1993). The hydrolytic water molecule in trypsin, revealed by time-resolved Laue crystallography. Science *259*, 669–673.
43. Brzozowski, A.M., et al., and Thim, L. (1991). A model for interfacial activation in lipases from the structure of a fungal lipase-inhibitor complex. Nature *352*, 491–494.
44. Sheffield, P., Garrard, S., and Derewenda, Z. (1999). Overcoming expression and purification problems of RhoGDI using a family of "Parallel" expression vectors. Protein Expr. Purif. *15*, 34–39.
45. Otwinowski, Z., and Minor, W. (1997). Processing of X-ray diffraction data collected in oscillation mode. Methods Enzymol. A *276*, 307–326.
46. Esnouf, R.M. (1997). BOBSCRIPT: an extensively modified version of MOLSCRIPT that includes greatly enhanced coloring capabilities. J. Mol. Graph. Model. *15*, 132–143.
47. Carson, M. (1991). Ribbons 2.0. J. Appl. Cryst. *24*, 958–961.
48. Nicholls, A., Sharp, K., and Honig, B. (1991). Protein folding and association: insights from the interfacial and thermodynamic properties of hydrocarbons. Proteins *11*, 281–296.
49. Jones, T.A., Zou, J.Y., Cowan, S.W., and Kjeldgaard, M. (1991). Improved methods for binding protein models in electron density maps and the location of errors in these models. Acta Cryst. A *47*, 110–119.
50. Sheldrick, G.W. (1997). SHELX-97, Gottingen University, Gottingen, Germany. http://shelx.uni-ac.gwdg.de/SHELX/.

Accession Numbers

Coordinates have been deposited with the Protein Data Bank (accession code 1FJ2); the GenBank accession code for the sequence of the construct used in this study is AF291053.